Supporting Information

Multifunctional pyrazino[2,3-*g*]quinoxaline derivative capable of acidochromic response, cancer cell imaging, and as an active layer for organic light-emitting diodes

Neichoihoi Lhouvum,[a] Sosmitha Girisa,[b] Anil Kumar,[c] Vinod Kumar Vishwakarma,[a] Abhishek Rameshchandra Tiwari,[a] Ajaikumar Bahulayan Kunnumakkara*[b], Jwo-Huei Jou,*[c] Achalkumar Ammathnadu Sudhakar*[a,d]

[a]*Department of Chemistry, Indian Institute of Technology Guwahati, Guwahati, 781039, Assam, India.*
[b]*Department of Biosciences and Bioengineering, Indian Institute of Technology Guwahati, Guwahati, 781039, Assam, India.*
[c]*Department of Materials Science and Engineering, National Tsing Hua University, No. 101, Section 2, Guangfu Rd., East District, Hsinchu, Taiwan, 30013*
[d]*Centre for Sustainable Polymers, Indian Institute of Technology Guwahati, Guwahati, 781039, Assam, India.*

Email addresses: achalkumar@iitg.ac.in**,** kunnumakkara@iitg.ac.in, jjou@mx.nthu.edu.tw

Table of Contents

1. Materials and Methods

Commercially available chemicals were utilized as received, and solvents were dried following standard procedures. Column chromatography was conducted using either silica gel (60–120 mesh or 100–200 mesh) or neutral aluminum oxide as the stationary phase. Thin-layer chromatography was performed using aluminum sheets pre-coated with silica gel as the stationary phase. IR spectra were recorded at room temperature on a PerkinElmer Universal ATR Two FT-IR spectrometer, with spectral positions reported in wavenumbers (cm^{-1}). NMR spectra were acquired using a Bruker 600 MHz NMR spectrometer (Make: Bruker, Model: AVANCE III HD). The chemical shifts in the ^{1}H NMR spectra were referenced to TMS as the internal standard and are reported in ppm while the coupling constants are given in Hz. Mass spectra were obtained using a MALDI-TOF mass spectrometer (Matrix Assisted Laser Desorption Ionization- Time Of Flight, Make: BRUKER Model: AUTOFLEX SPEED) with α-Cyano-4-hydroxycinnamic acid used as the matrix. The birefringence and fluidity properties of the final compounds were investigated using a polarizing optical microscope (Nikon Eclipse LV100POL) equipped with a programmable hot stage (Mettler Toledo FP90). Clean glass slides and cover slips were used for the polarizing optical microscopy studies. Transition temperatures and corresponding enthalpy changes were determined using a differential scanning calorimeter (Mettler Toledo DSC1) under a nitrogen atmosphere. The transition temperatures determined from calorimetric measurements during the heating and cooling cycles at a rate of 5 °C min^{-1} are recorded. Variable temperature XRD studies were performed on samples contained in Lindemann capillaries. Data were collected using a high-resolution X-ray powder diffractometer (PANalytical X'Pert PRO) equipped with a fast PIXCEL detector. Sample temperature was regulated with a Mettler hot stage/programmer (FP82HT/FP90). Thermogravimetric analysis (TGA) was performed on a Mettler Toledo thermogravimetric analyzer (model TG/SDTA 851e) under a nitrogen atmosphere, with a heating rate of 10 °C min^{-1}. UV-Vis spectra were recorded with a Perkin-Elmer Lambda 365+ UV/VIS/NIR spectrometer, while fluorescence emission measurements in solution state were recorded using a Horiba Fluoromax-4 fluorescence. Cyclic voltammetry studies were conducted using a Metrohm Autolab PGSTAT204 electrochemical workstation, operated with NOVA software.

2. Experimental Section

Scheme 1.

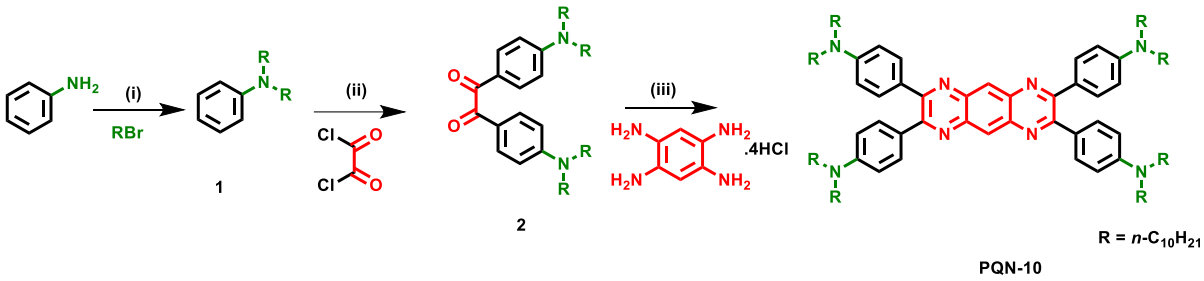

Reagents and conditions: (i) K_2CO_3, DMF, reflux, 24 hours, 86%; (ii) 1,2-dichloroethane, anhydrous $AlCl_3$, 0 °C, 30 min., RT, 17 hours, 45%; (iii) methanol: acetic acid (1:3), 130 °C, triethylamine, 12 hours, 75%.

Synthesis of *N,N*-didecylaniline(1)[1]

A mixture of aniline (3 mL, 32.9 mmol, 1 equiv.) and anhydrous K_2CO_3 (144.8 mmol, 4.4 equiv.) was taken in dry DMF (35 mL) and stirred for 1 hour at 60 °C. After that, *n*-bromodecane (120.8 mmol, 3.7 equiv.) was added and the mixture was refluxed for 24 hours under a nitrogen atmosphere. A blue colour appeared during the reaction but slow fades away with time. The solid residues were removed by filtration followed by removal of solvent in vacuo. The crude product was then reconstituted in DCM, washed with water and the organic fraction was dried over anhydrous Na_2SO_4. Removal of solvent in vacuo afforded a golden oil. The crude product was purified by column chromatography on silica gel (100-200 mesh). Elution with hexanes, followed by 5–10% ethyl acetate in hexanes, afforded the desired product as light yellow oil.

1: R_f = 0.65 (100% Hexane); light yellow liquid, yield: 86%; IR ν_{max} in cm^{-1}: 2922, 2852, 1741, 1598, 1503, 1463, 1366, 1192, 1114, 1037, 990, 856, 742, 690, 508; ^1H NMR (600 MHz, $CDCl_3$, 299 K): 7.23-7.20 (t, J = 7.8 Hz, 2H, H_{Ar}), 6.66-6.62 (m, 3H, H_{Ar}), 3.27-3.25 (t, 4H, 2× CH_2), 1.59 (m, 4H, 2× CH_2), 1.33-1.30 (m, 28H, 14 × CH_2), 0.92-0.90 (t, 6H, 2× CH_3); ^{13}C NMR (150 MHz, $CDCl_3$, 298.1K): 148.18, 129.17, 115.03, 111.66, 51.06, 31.91, 29.70, 29.60, 29.57, 29.35, 27.25, 27.22, 22.70, 14.13.

Synthesis of 1,2-bis(4-(didecylamino)phenyl)ethane-1,2-dione (2)[2,3]

To a 250 ml two necks dried round-bottom flask (RB) under argon atmosphere containing the solution of *N,N*-didecylaniline (8.03 mmol, 1.0 equiv.) in 1,2-dichloroethane (40 mL), was added oxalyl chloride (0.41 ml, 4.82 mmol, 0.6 equiv.) by syringe at 0 °C. The reaction mixture was kept at 0 °C for 10 min, and then anhyd. $AlCl_3$ (4.01 mmol, 0.5 equiv.) was added. After 30 min at 0 °C, the reaction mixture was allowed to reach room temperature and stayed overnight. The reaction mixture was then poured into 100 mL HCl (1M) solution. The organic layer was then extracted twice with dichloromethane (DCM), dried with anhydrous sodium sulphate, and concentrated. This crude product was purified in column

chromatography with silica gel and eluted with 50% DCM-hexane to get the pure product. Removal of solvent yielded the product **2**.

2: R_f = 0.52 (50% DCM-Hexane); greenish brown liquid, yield: 45%; IR ν_{max} in cm^{-1}: 2922, 2852, 1652, 1586, 1547, 1524, 1462, 1405, 1365, 1244, 1160, 1000, 880, 821, 769, 725, 698, 604, 510, 418; ^{1}H NMR (600 MHz, $CDCl_3$, 299 K): 7.82-7.81 (d, *J* = 8.4 Hz, 4H, H_{Ar}), 6.58-6.56 (d, *J* = 9.0 Hz, 4H, H_{Ar}), 3.32-3.30 (t, 8H, 4 × CH_2) , 1.58 (m, 8H, 4 × CH_2), 1.31-1.26 (m, 56H, 28 × CH_2), 0.89-0.87 (t, 12H, 4 × CH_3); ^{13}C NMR (150 MHz, $CDCl_3$, 298.1K): 193.73, 152.43, 132.45, 120.92, 110.54, 51.09, 31.88, 29.60, 29.54, 29.45, 29.30, 27.17, 27.04, 22.68, 14.12; MALDI-TOF exact mass calculated for $C_{54}H_{92}N_2O_2$ (M): 800.716, found: 800.865.

Synthesis of 4,4',4'',4'''-(pyrazino[2,3-*g*]quinoxaline-2,3,7,8-tetrayl)tetrakis(*N*,*N*-didecylaniline) (PQN-10)[3,4]

Compound **2** (0.40 g, 0.55 mmol, 2.1 equiv.) and benzene-1,2,3,4-tetraamine tetrahydrochloride (0.075 g, 0.26 mmol, 1.0 equiv.) were transferred into a 100 mL two neck RB flask with 8 mL methanol and 24 mL acetic acid (1:3) under argon atmosphere, which was heated to 100 °C. After the addition of 1.0 mL of triethylamine. The oil bath was maintained at 130 °C to ensure the continuous reflux of the reaction mixture was for 12 hours. Later the reaction mixture was concentrated. The crude product was purified by column chromatography on neutral alumina with 5-10% ethylacetate-hexane to yield an orange solid product (**PQN-10**).

PQN-10: R_f = 0.58 (10% EtOAc-Hexane); reddish purple solid, yield: 75%; IR ν_{max} in cm^{-1}; 2921, 2851, 1742, 1599, 1518, 1461, 1400, 1365, 1333, 1251, 1193, 1164, 1038, 964, 875, 820, 723, 646, 626, 599, 534, 418; ^{1}H NMR (600 MHz, $CDCl_3$, 299 K): 8.68 (s, 2H, H_{Ar}), 7.61-7.59 (d, *J* = 8.4 Hz, 8H, H_{Ar}), 6.61-6.59 (d, *J* = 8.4 Hz, 8H, H_{Ar}), 3.30-3.28 (t, 16H, 8 × N-CH_2), 1.59 (m, 16H, 8 × CH_2), 1.32-1.26 (m, 112H, 56 × CH_2), 0.90-0.87 (t, 24H, 8 × CH_3); ^{13}C NMR (150 MHz, $CDCl_3$, 298.1K): 154.48, 148.82, 140.14, 131.28, 126.41, 126.20, 110.99, 51.10, 31.91, 29.71, 29.59, 29.57, 29.34, 27.33, 27.20, 22.70, 14.13; MALDI-TOF exact mass calculated for $C_{114}H_{186}N_8$ (M): 1667.480, found (M+2): 1669.801.

3. NMR Spectra

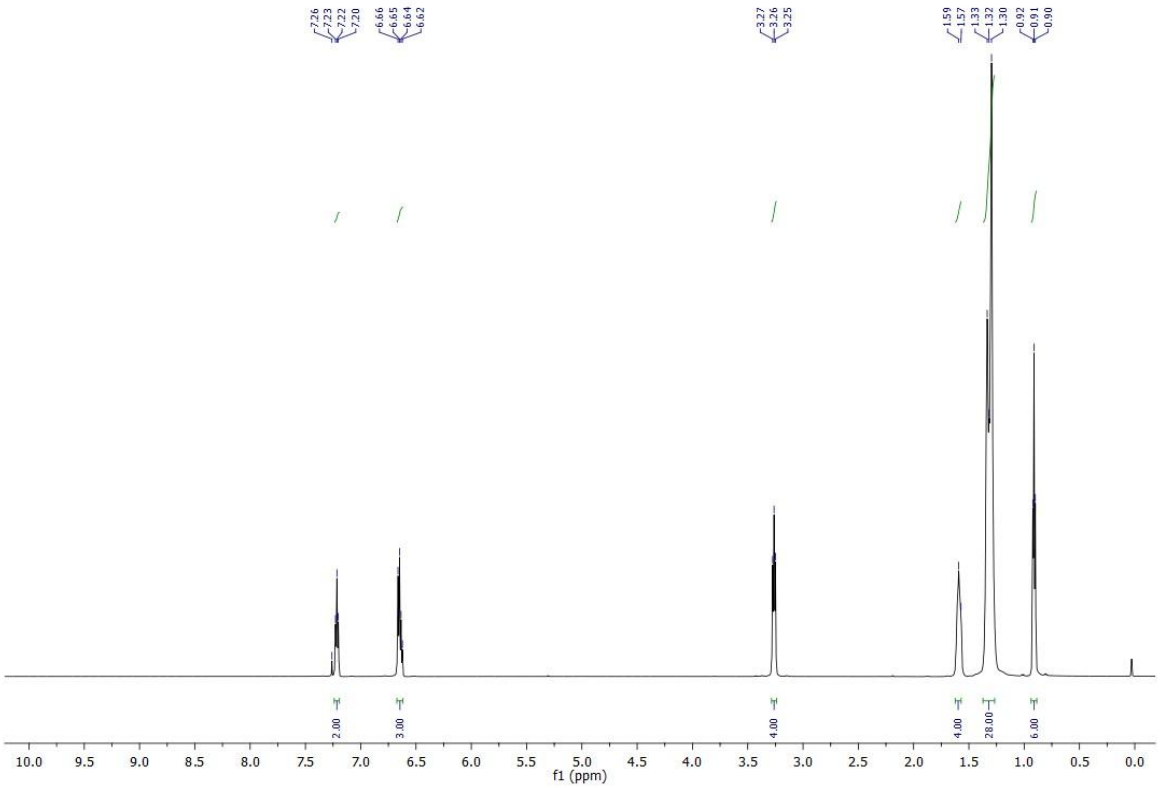

Figure S1. ^{1}H NMR (600 MHz) spectrum of **1** in $CDCl_3$.

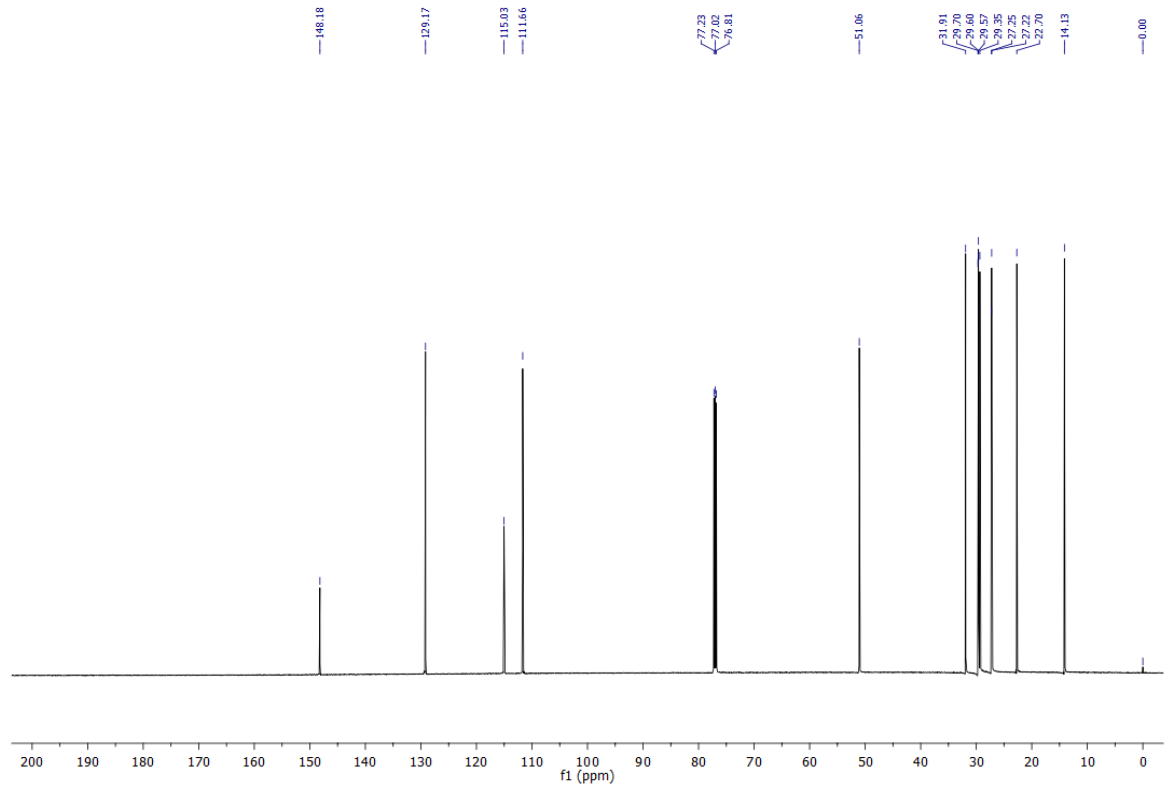

Figure S2. ^{13}C NMR (150 MHz) spectrum of **1** in $CDCl_3$.

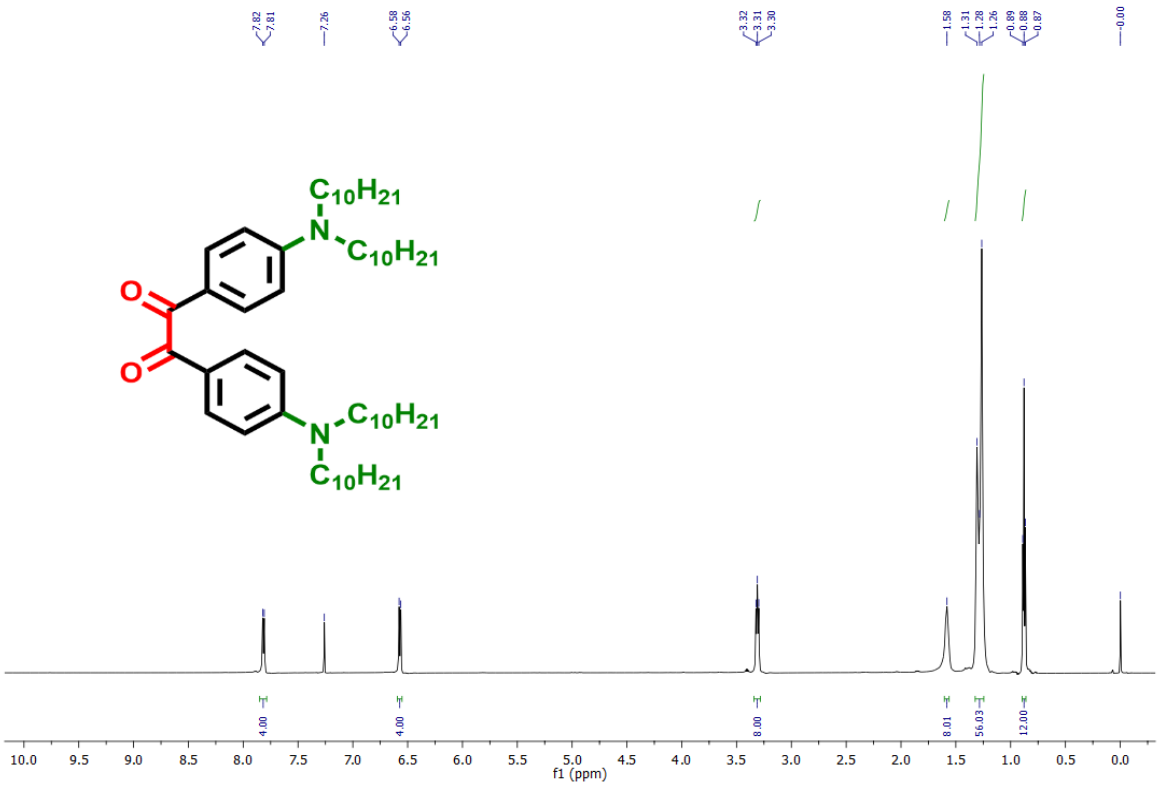

Figure S3. ^{1}H NMR (600 MHz) spectrum of **2** in $CDCl_3$.

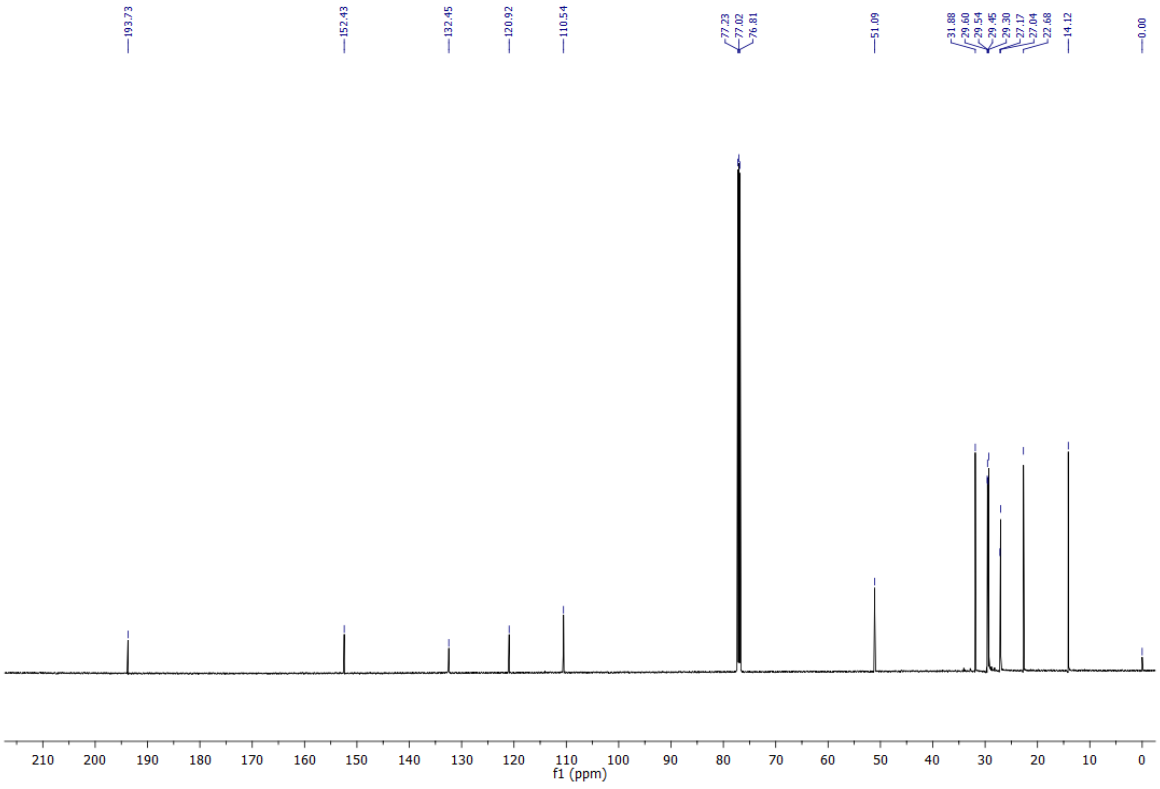

Figure S4. ^{13}C NMR (150 MHz) spectrum of **2** in $CDCl_3$.

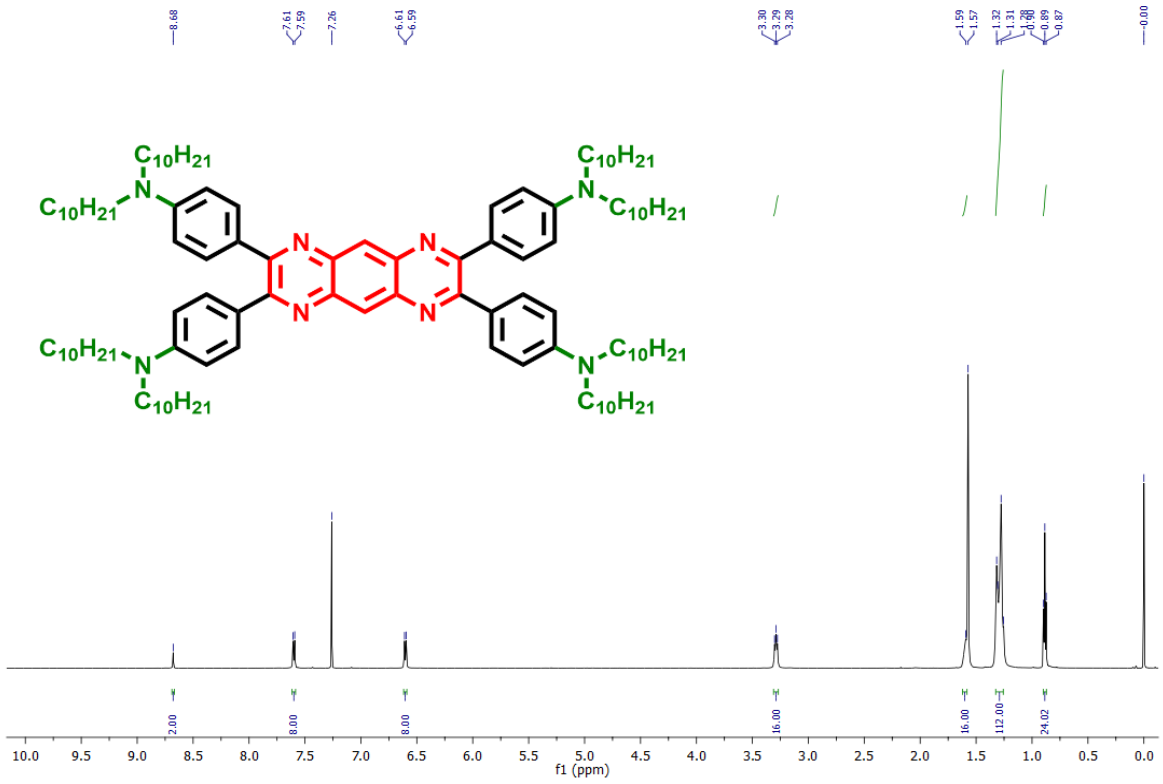

Figure S5. ^{1}H NMR (600 MHz) spectrum of **PQN-10** in $CDCl_3$.

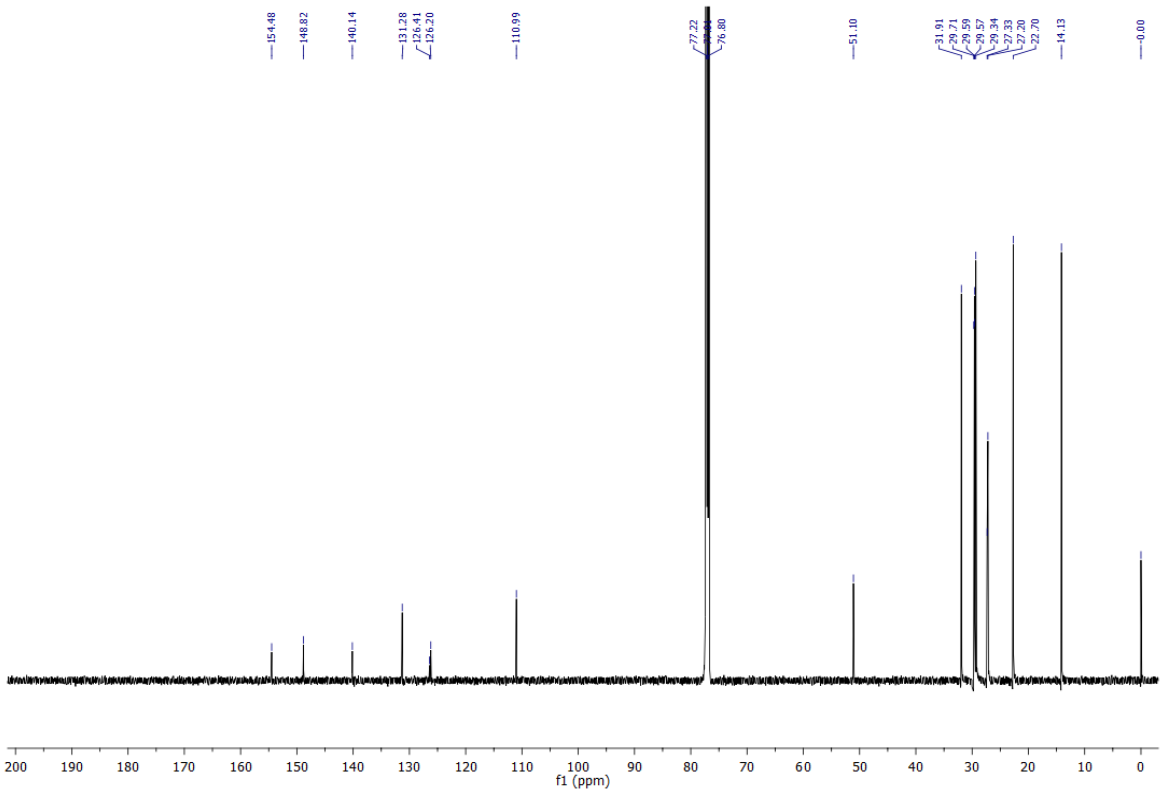

Figure S6. ^{13}C NMR (150 MHz) spectrum of **PQN-10** in $CDCl_3$.

4. MALDI-TOF Mass Spectra

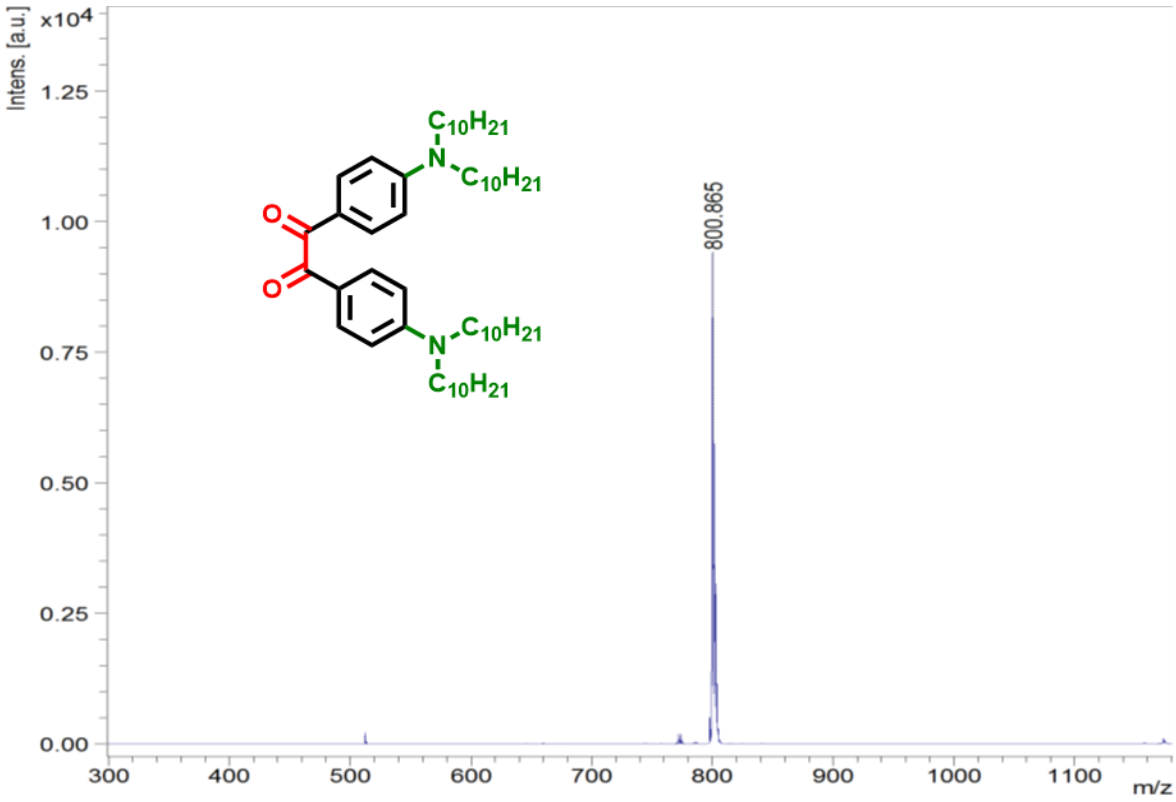

Figure S7. MALDI-TOF mass spectrum of compound **2**.

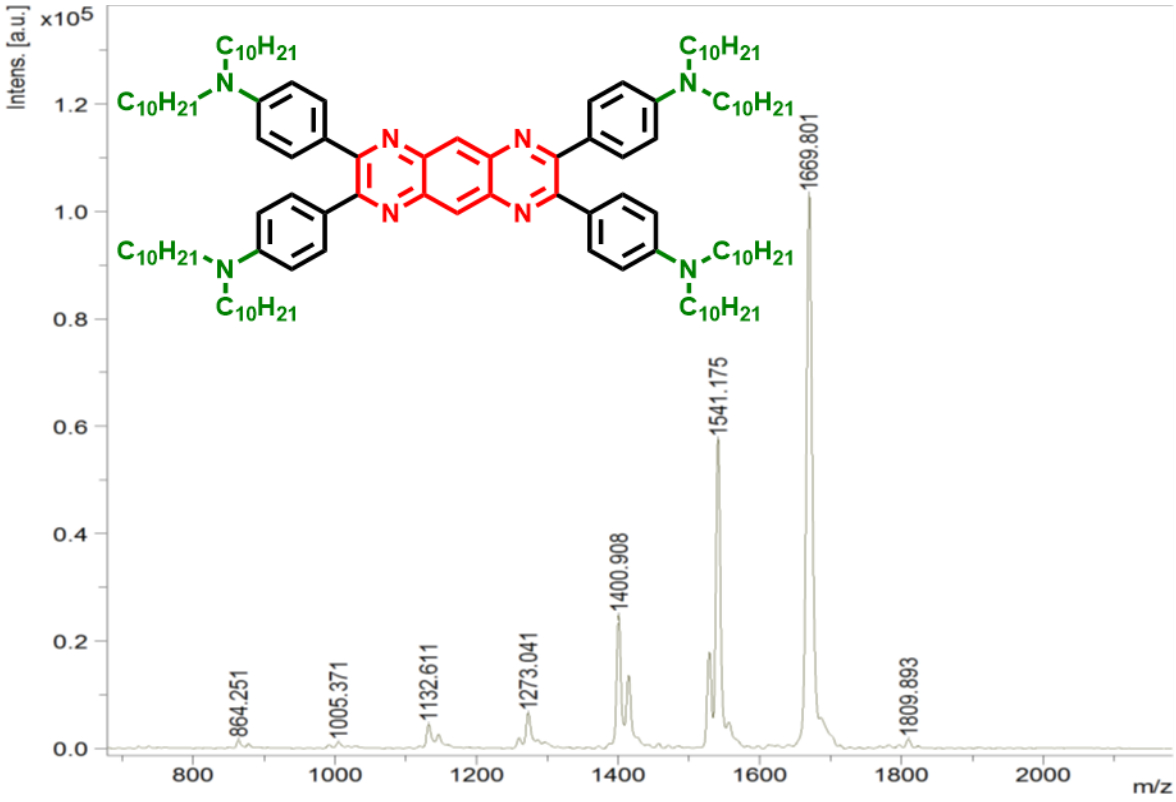

Figure S8. MALDI-TOF mass spectrum of compound of **PQN-10**.

5. Thermogravimetric Analysis

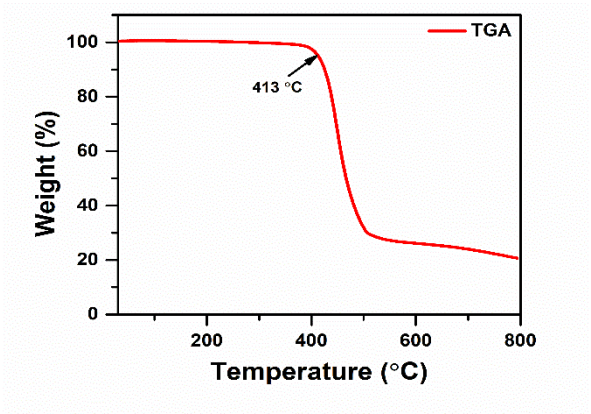

Figure S9. TGA thermogram of the compound **PQN-10** at a scan rate of 10 °C min^{-1} under N_2 atmosphere.

6. Polarized Optical Microscopy (POM)

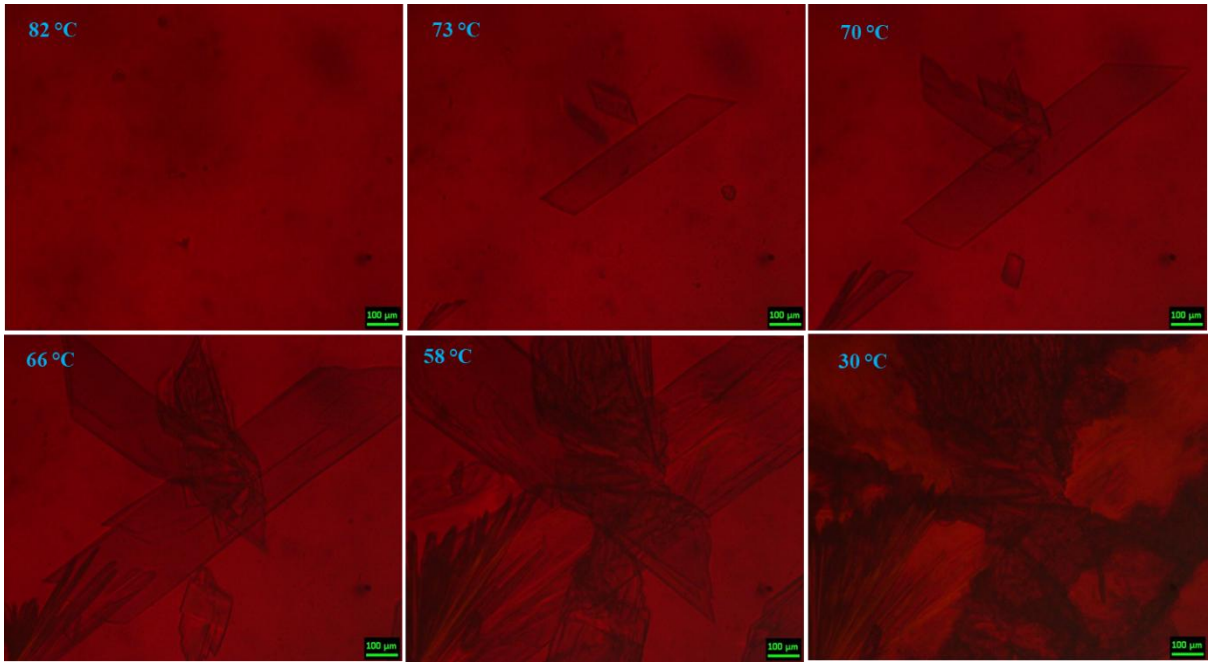

Figure S10. POM images of compound **PQN-10** on cooling the isotropic melt at a rate of 5 °C min^{-1}.

7. Differential Scanning Calorimetry (DSC)

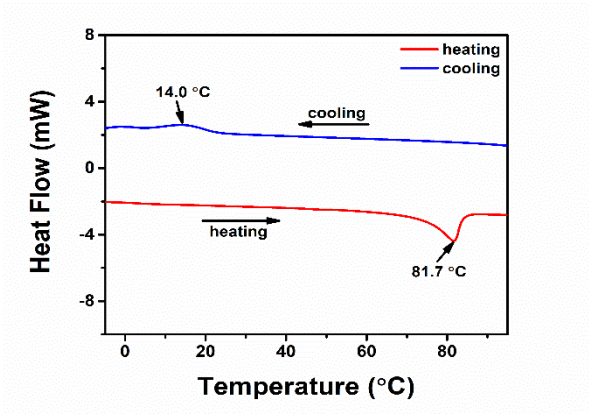

Figure S11. DSC traces obtained for compound **PQN-10** in the first cooling and second heating scans at a rate of 5 °C min^{-1} under the Nitrogen gas atmosphere.

Table S1. Phase transition temperatures[a] (°C) and corresponding enthalpies (kJ mol^{-1}) of compound **PQN-10.**

Entry	Phase Sequence (kJ/mol)[a]		T_5[b] (°C)
	Second heating	First Cooling	
PQN-10	Cr 81.7 (42.1) I	I[c] 73.0 Cr_1 14.0 (11.7) Cr_2	413
[a]Peak temperatures in the DSC thermograms obtained during the second heating and first cooling cycles at 5 °C min^{-1}; Cr = Crystalline phase; I = Isotropic phase. [b]Temperature at which 5 wt% decomposition was observed in TGA. [c]Transition observed in POM but enthalpy change non-detectable in DSC.			

8. Photophysical Properties

8.1. Aggregation Studies

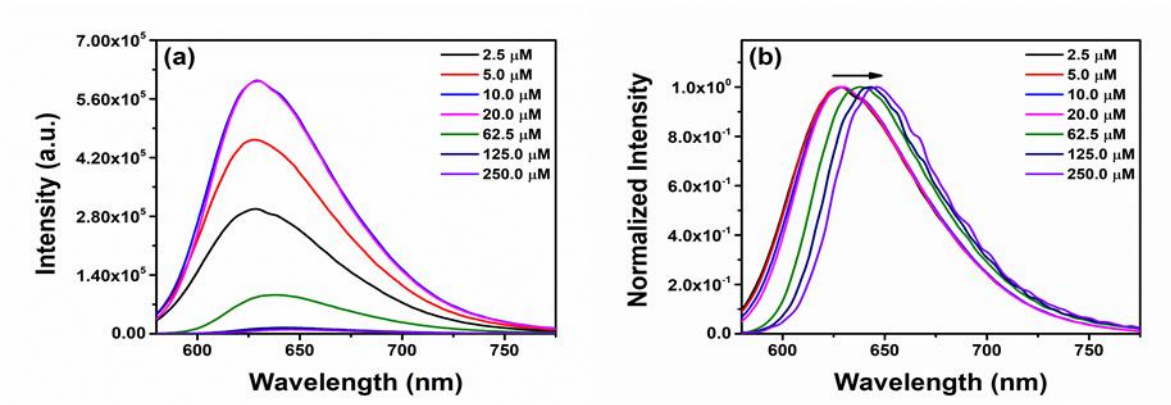

Figure S12. Emission spectra and normlalized emission spectra of compound **PQN-10** in high micromolar dichloromethane solutions.

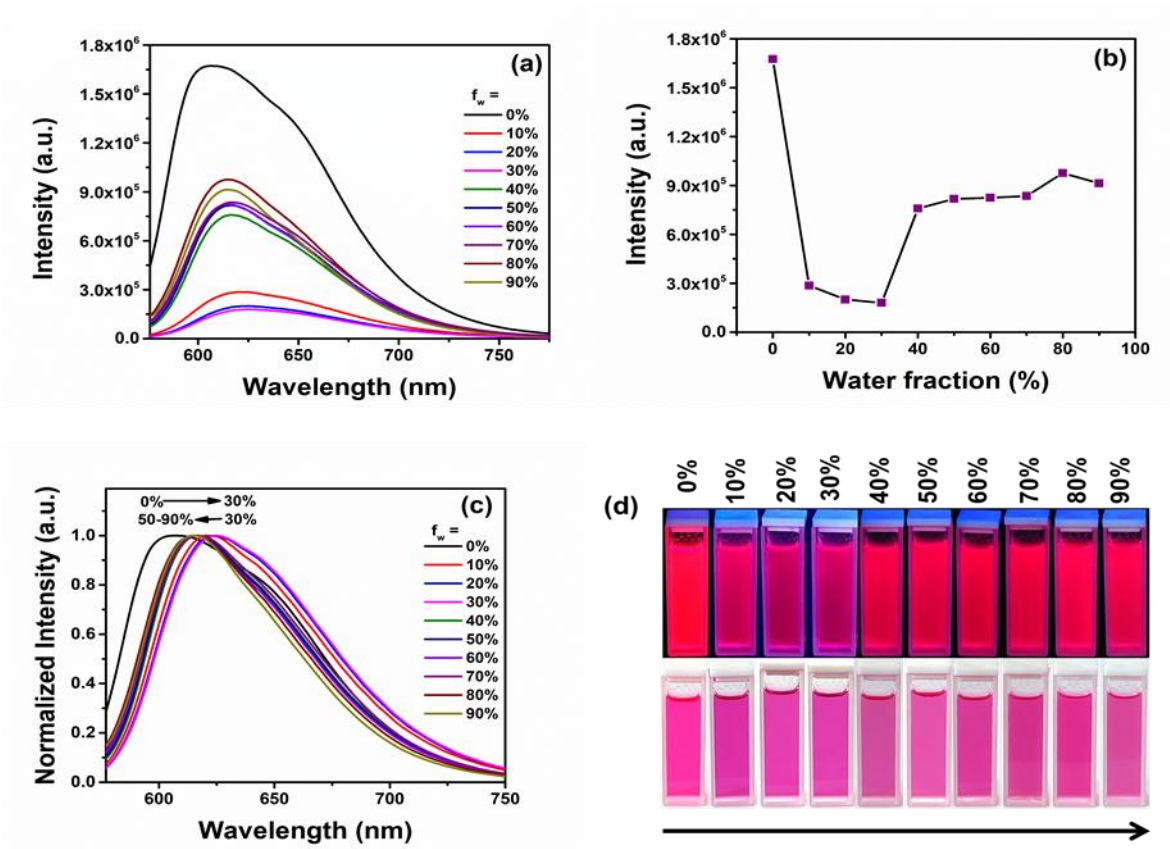

Figure S13. PL spectra of **PQN-10** (1.5×10^{-5} M) in Water/THF mixtures with different water fractions (a); Changes in PL peak intensity with water fraction (b); Normalized PL spectra of **PQN-10** (1.5×10^{-5} M) in Water/THF mixtures with different water fractions (c); Photographs of compound **PQN-10** under UV-light (above) and day-light (below) in THF-water upon increasing water fraction from f_w = 0 to 90% (d) (The direction of the arrow indicates the increase in water %).

8.2. Solvatochromism

Absorption and emission spectra were studied in solvents of varying polarity (from decane to acetone). No significant change in the peak maxima and the shape of the absorption band was noticed on varying the solvent polarity. The steady state emission spectra of compound **PQN-10** exhibited solvatochromic fluorescence on varying the polarity of solvents. A red-shifted absorption band and ACQ with a red-shifted emission were noticed in this solvent-dependent experiments. The emission spectra overlay reveals a red shift when transitioning from non-polar to polar solvents (yellow to purple emission). Notably, solvents such as dichloromethane, and chloroform exhibit a more pronounced deviation from the general trend of increasing emission wavelength, resulting in a greater red-shifted emission. However, acetone has the most pronounced red-shifted emission and the greatest stoke shift value (Table S2, Figure S15). This phenomenon is generally called positive solvatochromism, which indicates that increasing the solvent polarity induces the dipolar stabilization of the excited state (Table S6).

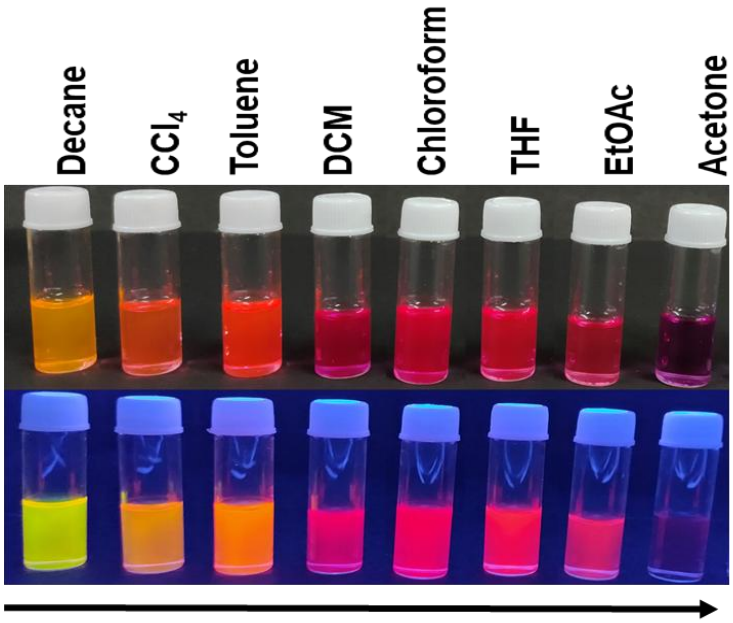

Figure S14. Photographs of compounds **PQN-10** taken under daylight and UV light in different solvents: Decane, Carbon tetrachloride, Toluene, Dichloromethane, Chloroform, Tetrahydrofuran, Ethyl acetate and Acetone in micromolar concentration (arrow indicates the lower to higher polarity order).

Table S2. Absorption and emission of compound **PQN-10** in different solvents

Solvents	**Absorption (nm)**	**Emission (nm)**	**Stokes Shift (cm^{-1})**
Decane	472, 502, 536	554, 589	620
Carbon tetrachloride	512, 547	568, 603	670
Toluene	520, 554	584	930
Dichloromethane	564	631	1900
Chloroform	567	622	1560
Tetrahydrofuran	533, 563	604	1190
Ethyl acetate	527, 554	600	1380
Acetone	567	645	2140

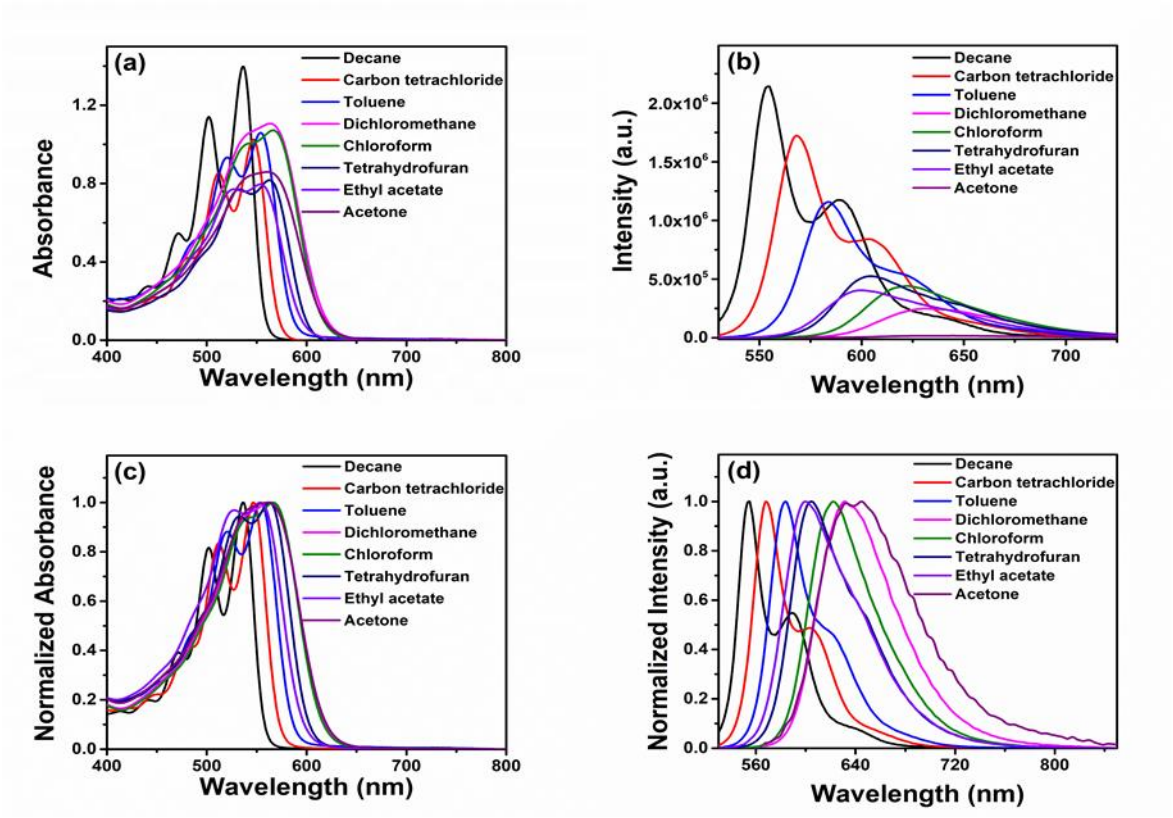

Figure S15. Solvatochromism study of compound **PQN-10**: Overlay of absorption spectra (a) and emission spectra (b); Normalized absorption spectra (c); and Normalized emission spectra (d). (Concentration: 10 µM).

8.3. Acidochromism

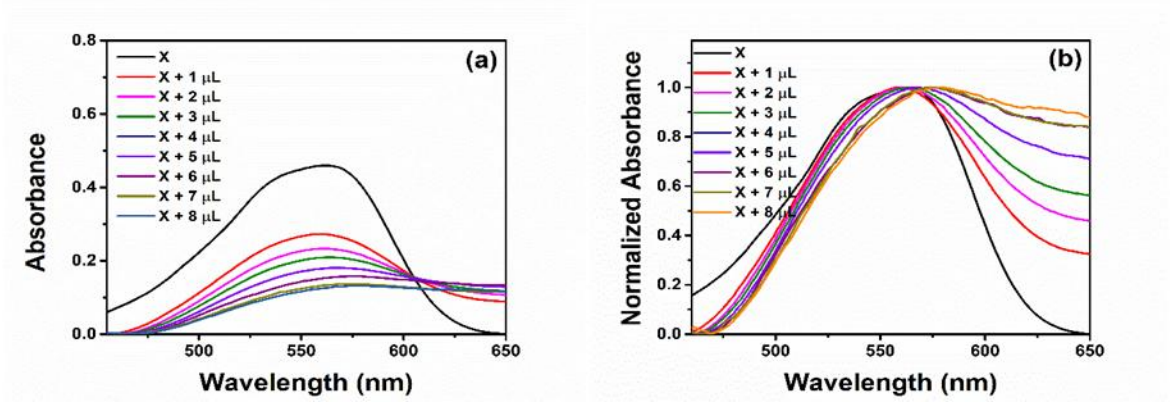

Figure S16. Absorption spectra (a) and Normalized Absorption spectra (b) of compound **PQN-10** on successive addition of 0.1 M TFA (1 µL to 8 µL) (X = 10 µM **PQN-10** in dichloromethane solution)

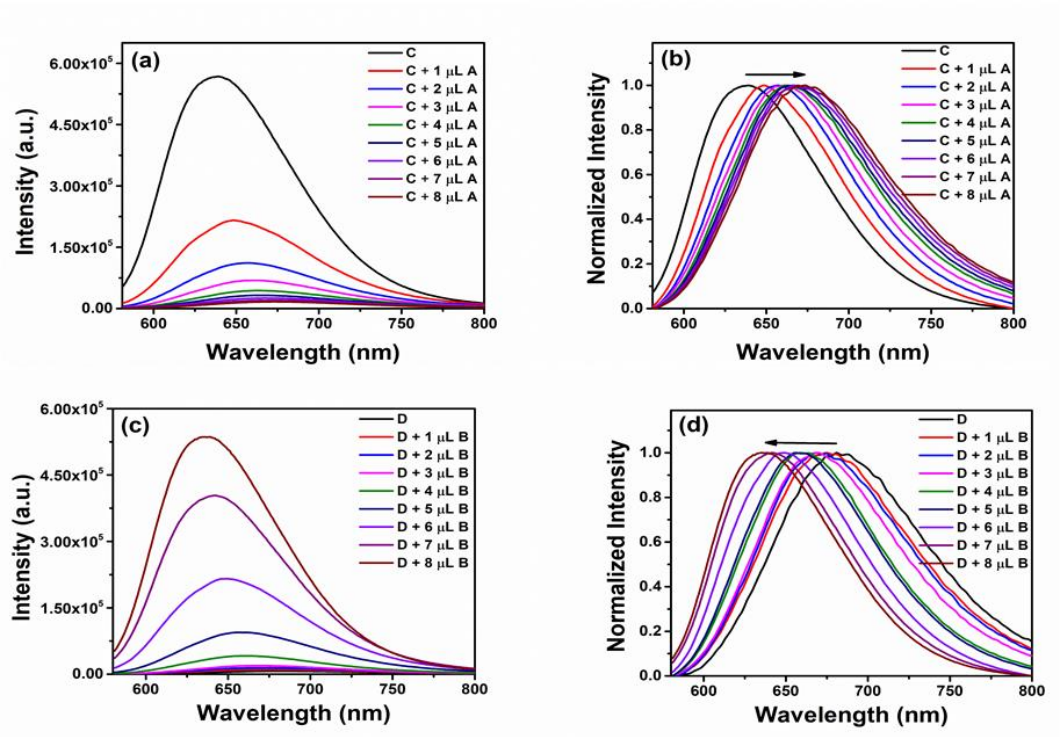

Figure S17: Emission spectra (a) and Normalized emission spectra (b) of compound **PQN-10** on the incremental addition of **A** (**C** is micromolar concentration of **PQN-10** and **A** is 0.5 M TFA); Emission spectra (c) and Normalized emission spectra (d) of **D** on the incremental addition of **B** (**D** is mixture of micromolar concentration of **PQN-10** with 10 μL of 0.5 M TFA and **B** is 0.5 M TEA).

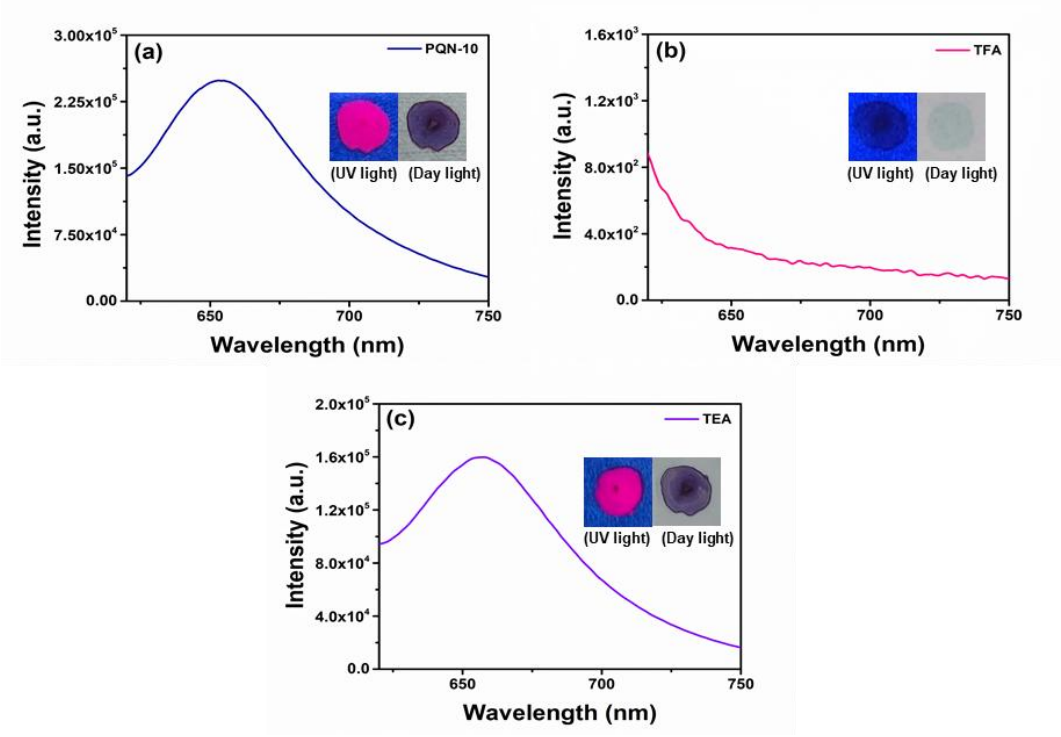

Figure S18. Emission spectrum of compound **PQN-10** in thin film before TFA vapour exposure (a); after exposure (b); and recovery of emission of compound **PQN-10** by neutralization with TEA vapour (c) (obtained by dropcasting 100 μM dichloromethane solution of compound **PQN-10** on to a quartz plate; Inset: Photographs of the thin film in UV light and day light).

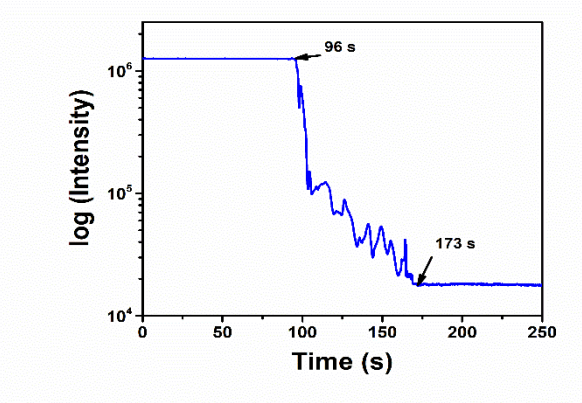

Figure S19. Semi-log plot of real-time fluorescence on addition of 10 μL of 0.5 M TFA solution to 10 μM dichloromethane solution of **PQN-10**.

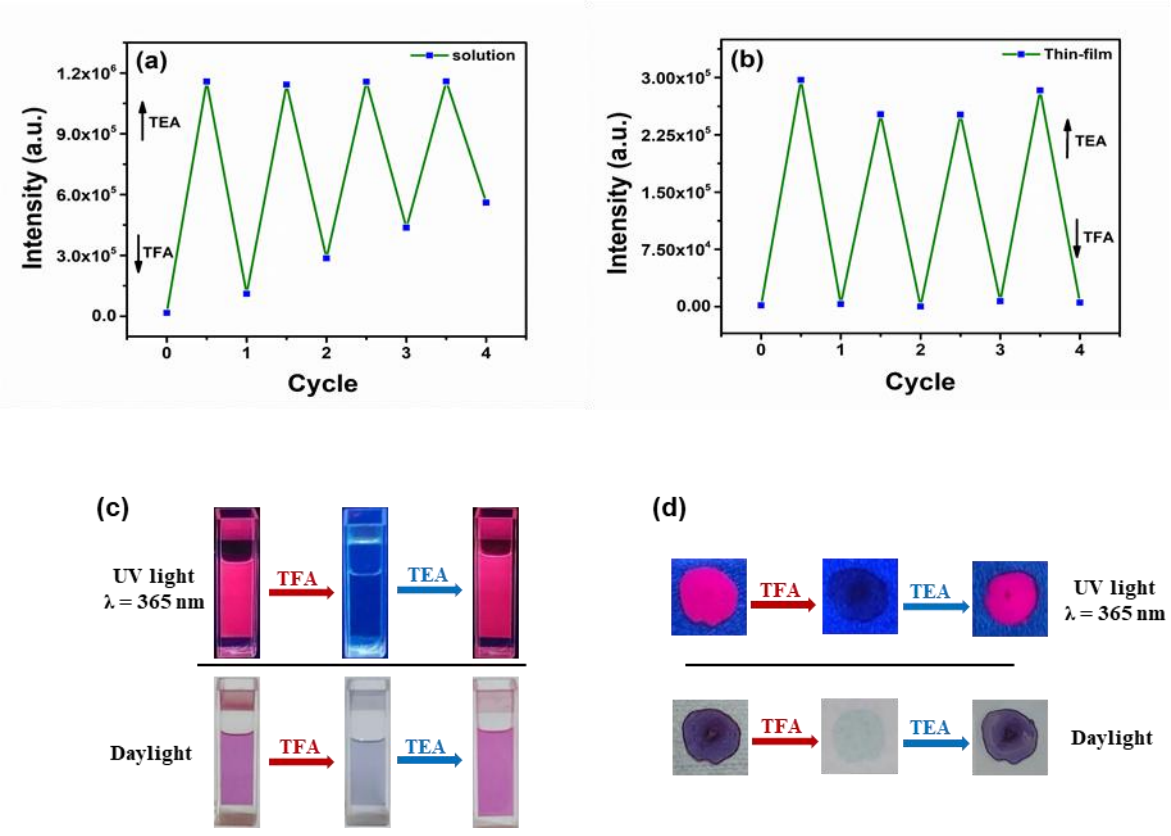

Figure 20. The fluorescence intensity upon consecutive addition or exposure of TFA and TEA for upto 4 cycles in dichloromethane solution (a); thin-film (b); photographs showing the response of the solution of compound **PQN-10** to TFA and TEA (c); drop casted film on a TLC plate (d), as seen under day light and UV light (λ= 365 nm).

Detection Limit

Samples of **PQN-10** (5 μM) with varying concentrations of TFA (0.0, 2.0, 4.0, 6.0 and 8.0 μM) were prepared in dichloromethane. Fluorescence spectra were recorded at an excitation wavelength of 564 nm for each sample. The change in fluorescence intensity was plotted against TFA concentration. This yielded a linear calibration curve with a correlation coefficient R = 0.99. The limit of detection (LOD) was calculated by the formula LOD = 3σ/K, where σ

is the standard deviation of the fluorescence intensity of **PQN-10** without TFA, and K is the slope of the linear regression line.

$LOD = 3 \times \sigma / K$
$LOD = 3 \times 20938.45 / 13783$
$= 4.56\ \mu M$ or **519.66 ppb**

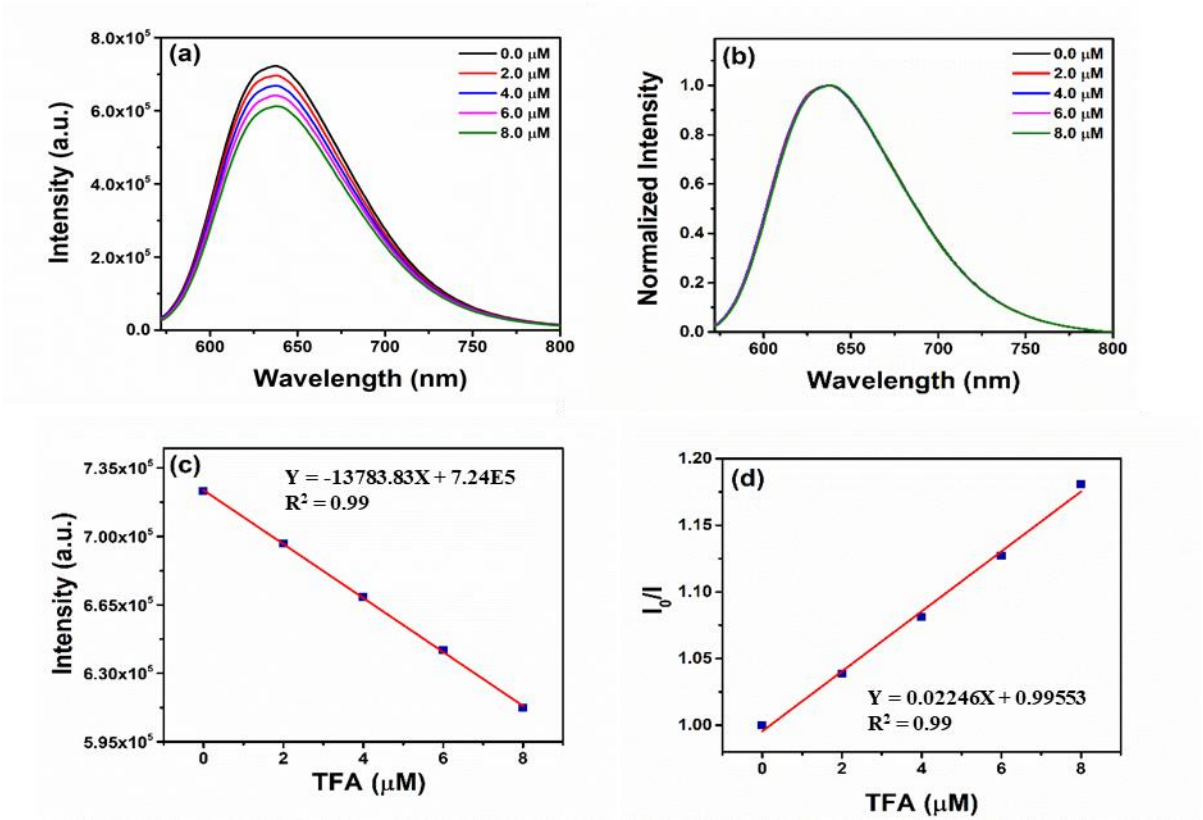

Figure S21. Fluorescence response of compound **PQN-10** (5 μM) in dichloromethane on incremental addition of TFA solution (a); Normalized version of the fluorescence response (b); Plot showing the variation of fluorescence intensity of compound **PQN-10** (5 μM) in dichloromethane on addition of TFA (c); Stern-Volmer plot obtained for the same (d).

Table S3. LOD for TFA of some quinoxaline derivatives.[5–7]

Sl. No.	Compound	LOD (ppm)
1.	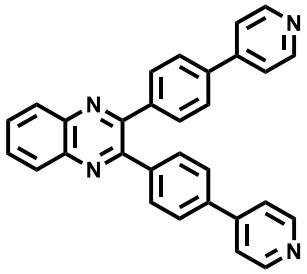	0.0333 (M. Lamoria, D. Manna, M. D. Milton, *J. Mol. Struct.* 2025, **1319**, 139385.)

2.	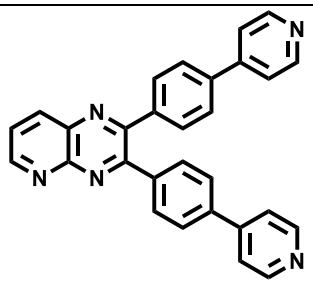	0.0173 (M. Lamoria, D. Manna, M. D. Milton, *J. Mol. Struct.* 2025, **1319**, 139385.)
3.	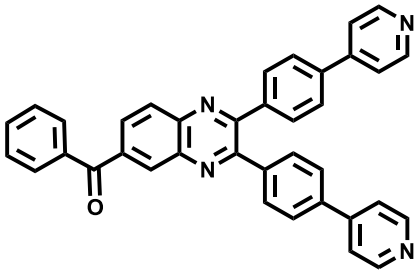	0.500 (M. Lamoria, D. Manna, M. D. Milton, *J. Mol. Struct.* 2025, **1319**, 139385.)
4.	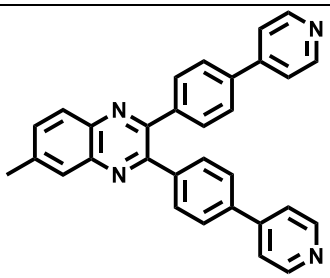	0.0478 (M. Lamoria, D. Manna, M. D. Milton, *J. Mol. Struct.* 2025, **1319**, 139385.)
5.	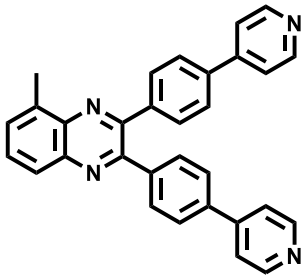	0.2304 (M. Lamoria, D. Manna, M. D. Milton, *J. Mol. Struct.* 2025, **1319**, 139385.)
6.	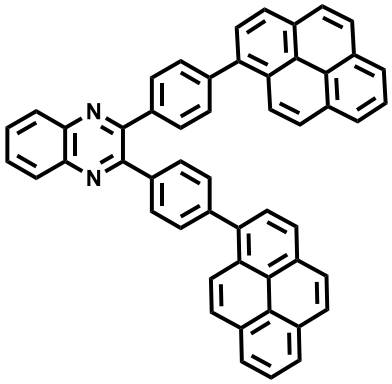	4.395 (M. Lamoria, M. D. Milton, *Dyes Pigm.* 2023, **213**, 111182.)

7.	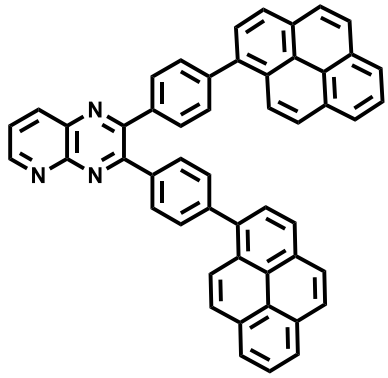	1.093 (M. Lamoria, M. D. Milton, *Dyes Pigm.* 2023, **213**, 111182.)
8.	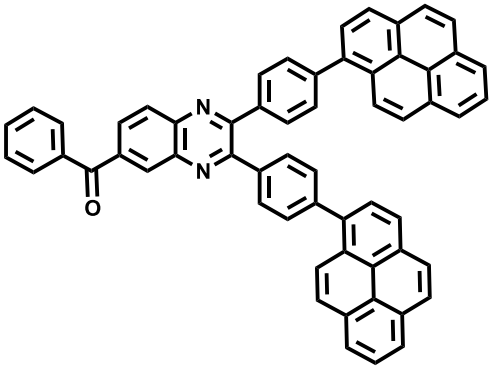	4.905 (M. Lamoria, M. D. Milton, *Dyes Pigm.* 2023, **213**, 111182.)
9.	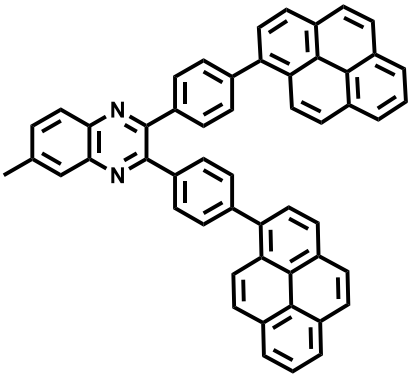	2.044 (M. Lamoria, M. D. Milton, *Dyes Pigm.* 2023, **213**, 111182.)
10.	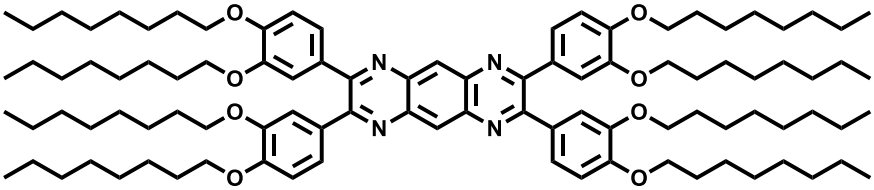	0.253 (V. K. Vishwakarma, V. Adupa, K. A. Reddy, A. A. Sudhakar, *J. Mol. Struct.* 2021, **1225**, 129120.)
11	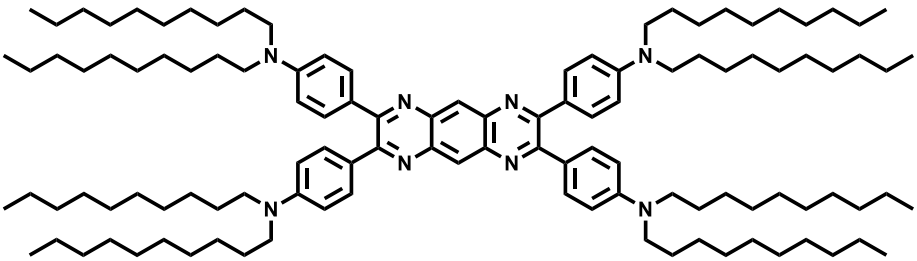	0.520 (This work)

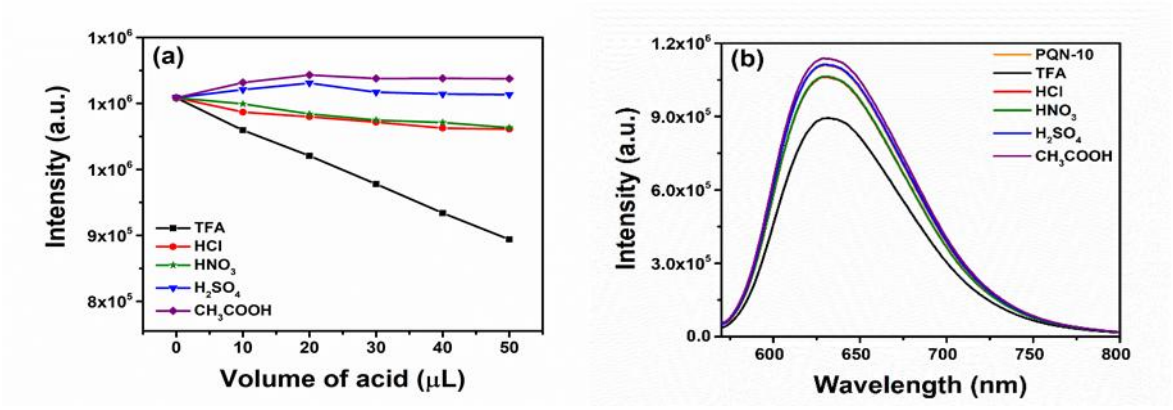

Figure S22. Plot of intensity vs volume of acid added of various acids (100 μM) in **PQN-10** (10 μM) dichloromethane solution (a); Emission spectrum of **PQN-10** (10 μM) on addition of 50 μL of 100 μM dichloromethane solution of acids (b).

8.4. Time Resolved Photoluminescence Spectroscopy (TRPL)

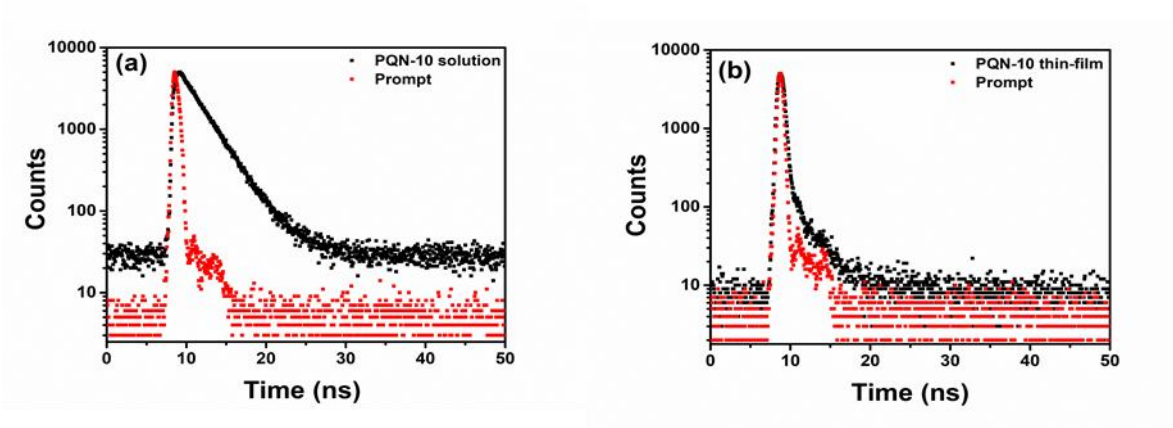

Figure S23. Fluorescence decay curves of **PQN-10** in micromolar dichloromethane solution (a) and in thin-film state (b).

Table S4. Data obtained from the time-resolved photoluminescence spectroscopy of **PQN-10** in dichloromethane solution and in thin-film state.

State	τ_1 (ns)	α_1 (%)	τ_2 (ns)	α_2 (%)	χ^2
DCM solution	2.78	100	-	-	1.08
Thin-film	0.29	28	2.70	72	1.15

The values of α and τ represent the relative percentage and lifetime of molecules.

9. Quantum yield measurement

The relative quantum yield of **PQN-10** was determined using rhodamine B in ethanol (Qf = 0.70) as the reference standard. Absolute value was calculated according to the following

equation: $Q_S = Q_R \times (m_S / m_R) \times (n_S / n_R)^2$ where, Q: Quantum yield; m: Slope of the plot of integrated fluorescence intensity *vs* absorbance; n: refractive index (1.446 for chloroform and 1.361 for ethanol). The subscript R designates the reference fluorophore (rhodamine B), while subscript S corresponds to the sample under investigation. To minimize re-absorption (inner filter) effects, the absorbance at the excitation wavelength of 566 nm was maintained below 0.12. The quantum yield of rhodamine B is 0.70. A simplified equation for the calculation after substituting the appropriate values is given below and values obtained are given in the table below.

$$Q_S = 0.70 \times (m_S / m_R) \times (1.446/1.361)^2$$

$$= 0.70 \times (m_S / m_R) \times 1.12881$$

Table S5. Relative quantum yield of the compound **PQN-10**

Compound	$\mathbf{m_S}$	$\mathbf{m_R}$	$\mathbf{Q_S}$ [a, b, c]
PQN-10	5.12486×10^6	7.20551×10^6	0.56

[a]Measured in chloroform.

[b]Excited at absorption maxima.

[c]Rhodamine B ($\mathbf{Q_f}$ = 0.70) in ethanol.

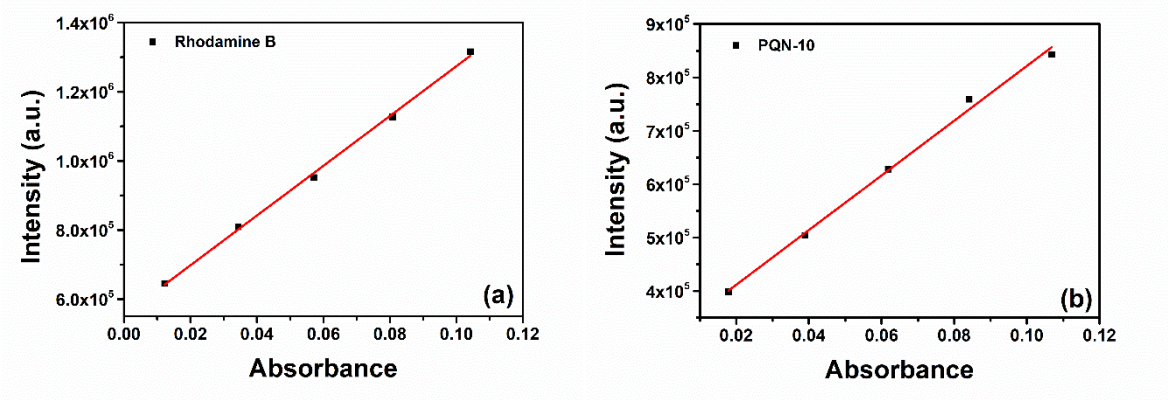

Figure S24. Plots of integrated photoluminescence intensity vs absorbance of Rhodamine B in ethanol solution excited at 566 nm (**Ref.**); integrated photoluminescence intensity *vs* absorbance of compound **PQN-10** in chloroform solution excited at 566 nm.

10. Cytotoxicity studies

MTT Assay Protocol

Cell viability was assessed using the 3-(4,5-dimethylthiazol-2-yl)-2,5-diphenyltetrazolium bromide (MTT) assay. The cells were seeded in a 96-well plate at a density of 2,000 cells per well and allowed to attach overnight under standard culture conditions. Following this, cells were treated with the indicated concentrations (0, 5, 10, 25, 50, 100 µM) of the compound. Control wells received vehicle only. Cells were incubated with the treatment for 0 h and 72 h. At the respective time points, MTT (5 mg/mL) was added to each well and incubated for 2 hours at 37ºC to allow the formation of for formazan crystals. The medium was then carefully

removed, and the formazan crystals were dissolved in DMSO solvent (100 µL per well). The absorbance was then measured at 570 nm using a microplate reader. Cell viability was calculated as a percentage relative to control.

Result:

The cytotoxicity of the compound was assessed using an MTT assay in cancer and normal cells following 72 h of treatment. In cancer cells, treatment with increasing concentrations of the compound resulted in a concentration-dependent decrease in cell viability. However, cells retained high viability (~90-96%) at lower concentrations (5-50 µM), while a moderate reduction to ~75-80% viability was observed at 100 µM. In contrast, normal cells exhibited no significant reduction in viability across the tested concentration range, indicating minimal cytotoxicity under similar conditions. Overall, these results demonstrate that the compound exhibits low cytotoxicity at imaging-relevant concentrations and preferential effects at higher doses in cancer cells, supporting its biocompatibility and suitability for bioimaging applications.

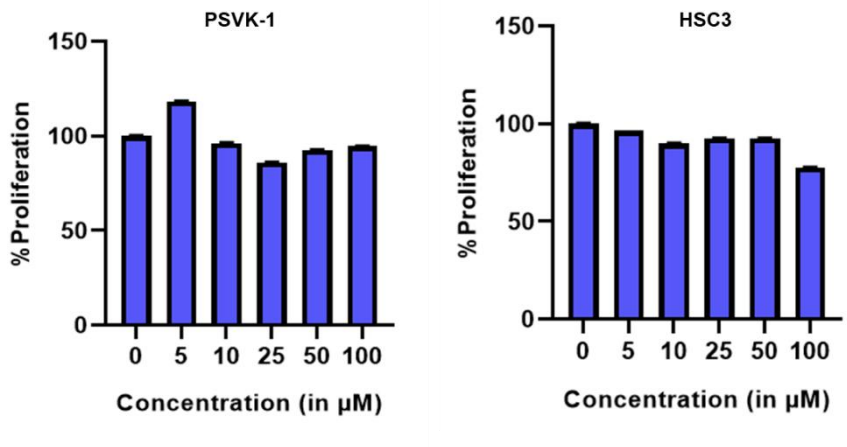

Figure S25. Cytotoxicity assessment of the compound by MTT assay in (A) PSVK-1 and (B) HSC3 cell lines. Cells were treated with increasing concentrations of the compound (0-100 µM) for 72 h following seeding at a density of 2,000 cells per well. Cell viability was measured and expressed as percentage relative to untreated control.

11. Theoretical Calculations

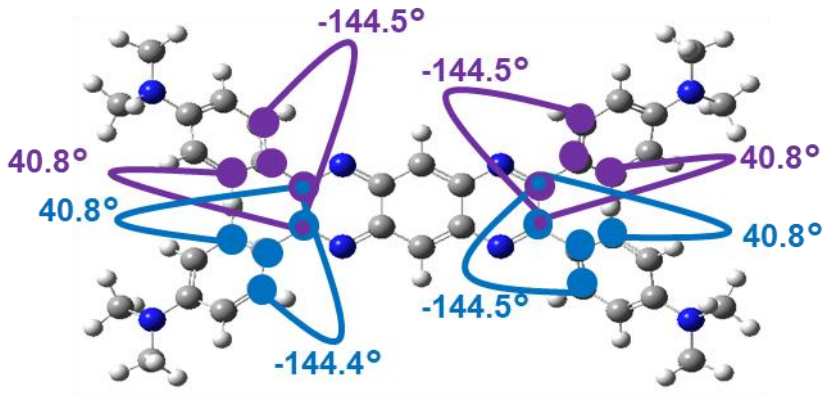

Figure S26. Optimized conformation and dihedral angles of the compound **PQN-10**.

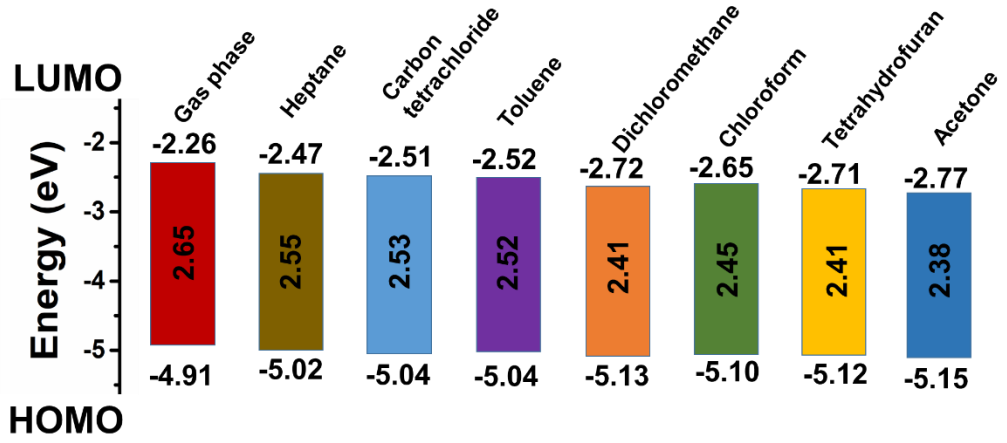

Figure S27. Schematic diagram showing the HOMO-LUMO levels, energy band-gap when performed in gaseous phase, heptane, carbon tetrachloride, toluene, dichloromethane, chloroform, tetrahydrofuran and acetone solvents. (TD-DFT studies were calculated at B3LYP/6-31G+(d,p), cpcm level).

Table S6. Optimization and TD-DFT studies of compound **PQN-10** were performed at B3LYP/6-31G+(d,p), cpcm* system (solvents are studied from non-polar to polar order).

(phase/solvents)	HOMO (eV)	LUMO (eV)	Eg (eV)	Absorption (nm)	S_1 (eV)	T_1 (eV)	ΔE_{ST} (eV)
Gaseous phase	-4.91	-2.26	2.65	539	2.29	1.76	0.53
Heptane*	-5.02	-2.47	2.55	576	2.14	1.77	0.37
Carbon tetrachloride*	-5.04	-2.51	2.53	581	2.12	1.77	0.35
Toluene*	-5.04	-2.52	2.52	584	2.11	1.76	0.35
Dichloromethane*	-5.13	-2.72	2.41	615	2.00	1.50	0.50
Chloroform*	-5.10	-2.65	2.45	601	2.05	1.76	0.29
Tetrahydrofuran*	-5.12	-2.71	2.41	609	2.02	1.73	0.29
Acetone*	-5.15	-2.77	2.38	620	1.97	1.69	0.28

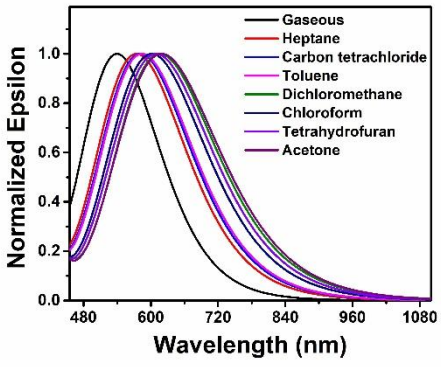

Figure S28. Schematic diagram showing the Normalized UV spectra when performed in gaseous phase, heptane, carbon tetrachloride, toluene, dichloromethane, chloroform, tetrahydrofuran and acetone solvents. (TD-DFT studies were calculated at B3LYP/6-31G+(d,p), cpcm level).

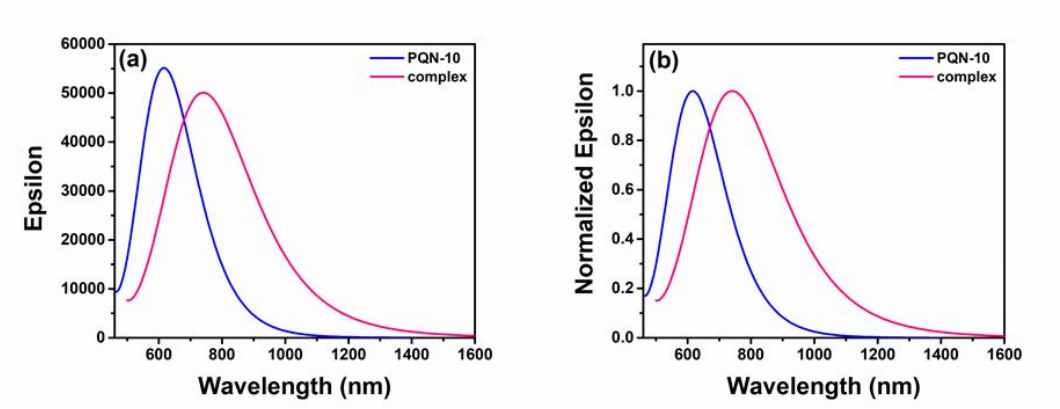

Figure S29. Schematic diagram showing the UVspectra (a) and Normalized UV spectra (b) of **PQN-10** and the complex (with **PQN-10** protonated at pyrazino[2,3-g]quinoxaline N) when TD-DFT studies were calculated at B3LYP/6-31+G(d,p), cpcm level, dichloromethane solvent.

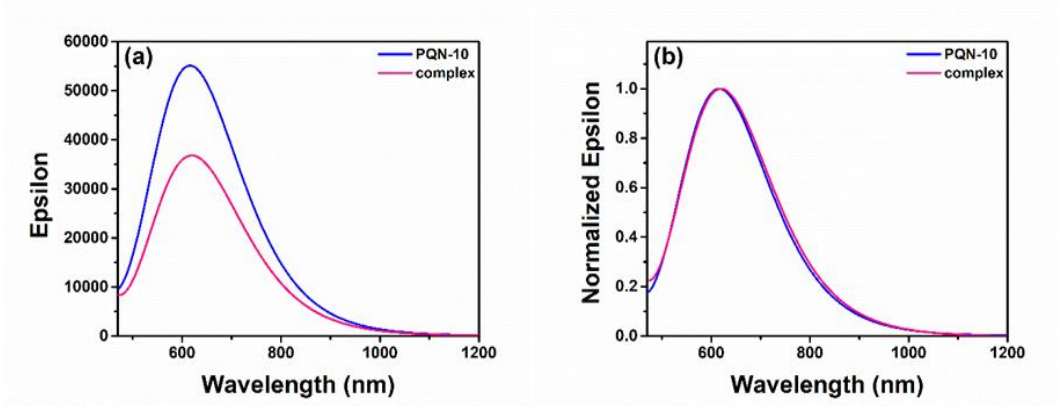

Figure S30. Schematic diagram showing the UVspectra (a) and Normalized UV spectra (b) of **PQN-10** and the complex (with **PQN-10** protonated at dialkylated aniline's N) when TD-DFT studies were calculated at B3LYP/6-31+G(d,p), cpcm level, dichloromethane solvent.

Compound name	HOMO	LUMO	HOMO-LUMO Energy gap (eV)	Energy (hartree)
TFA	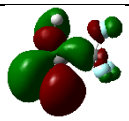 -3.13 eV	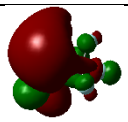 0.74 eV	3.87	-526.91
PQN-10 Protonated at aniline N	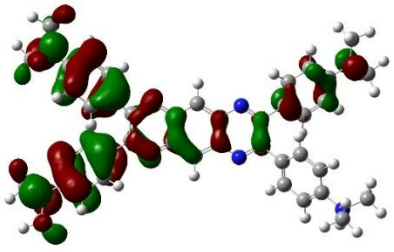 5.37 eV	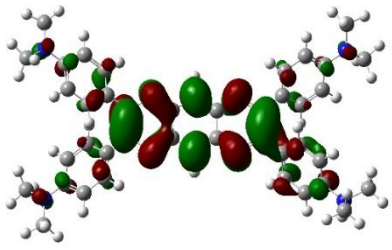 -3.07 eV	2.30	-2064.35

Complex (When PQN-10 is protonated at aniline N)	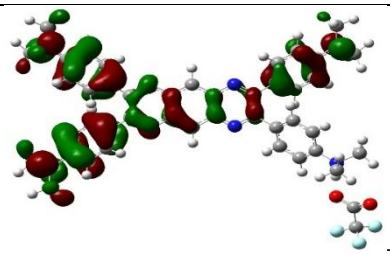 5.25 eV	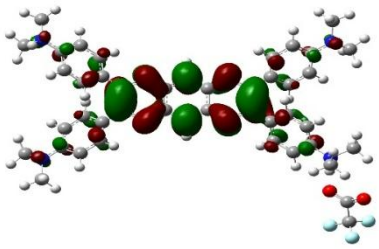 -2.89 eV	2.36	-2590.77
PQN-10 Protonated at core N	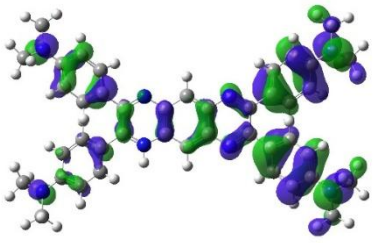 5.43 eV	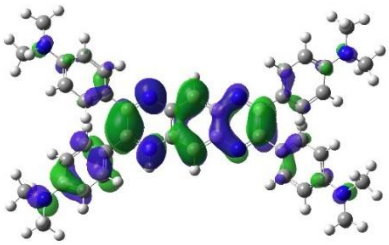 -3.72 eV	1.71	-2064.36
Complex (When PQN-10 is protonated at core N)	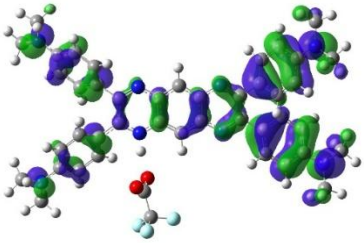 -5.23 eV	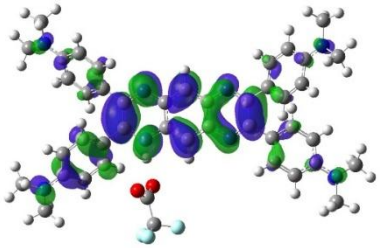 -3.29 eV	1.94	-2590.77

1 hartree = 2625.50 kJ mol^{-1}

Figure S31. HOMO and LUMO of deprotonated TFA and protonated **PQN-10** (at aniline N and core N) and the complex of both solvated in chloroform when **PQN-10** is protonated at aniline N and core N.

12. Electroluminescence studies

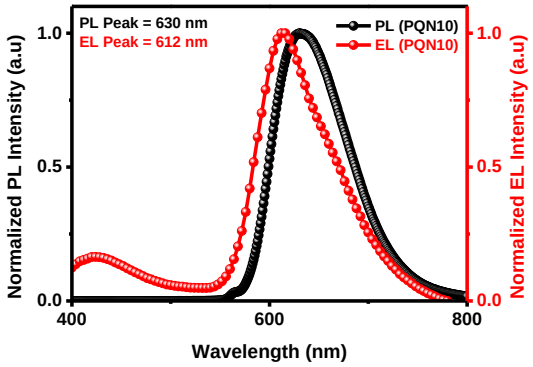

Figure S32. Photoluminescence and electroluminescence spectra overlap

13. References

1. K. D. Thériault, T. C. Sutherland, *Phys. Chem. Chem. Phys.* 2014, **16**, 12266-12274.
2. D. Kiymaz, M. Sezgin, E. Sefer, C. Zafer, S. Koyuncu, *Int. J. Hydrogen Energy* 2017, **42**, 8569-8575.

3. V. K. Vishwakarma, M. R. Nagar, N. Lhouvum, J.-H. Jou, A. A. Sudhakar, *Adv. Opt. Mater*. 2022, **10**, 2200241.
4. W. Liu, X. Luo, Y. Bao, Y. P. Liu, G.-H. Ning, I. Abdelwahab, L. Li, C. T. Nai, Z. G. Hu, D. Zhao, B. Liu, S. Y. Quek, K. P. Loh, *Nat. Chem*. 2017, **9**, 563-570.
5. M. Lamoria, D. Manna, M. D. Milton, *J. Mol. Struct.* 2025, **1319**, 139385.
6. M. Lamoria, M. D. Milton, *Dyes Pigm.* 2023, **213**, 111182.
7. V. K. Vishwakarma, V. Adupa, K. A. Reddy, A. A. Sudhakar, *J. Mol. Struct.* 2021, **1225**, 129120.